ESANN 2010 proceedings, European Symposium on Artificial Neural Networks - Computational Intelligence and Machine Learning. Bruges (Belgium), 28-30 April 2010, d-side publi., ISBN 2-930307-10-2.

A critique of BCM behavior verification for STDP-type plasticity models

Christian Mayr, Johannes Partzsch and Rene Schüffny *

Endowed Chair of Highly-Parallel VLSI-Systems and Neural Microelectronics,
University of Technology Dresden, Dresden, Germany

Abstract. Rate based (Bienenstock-Cooper-Munroe, BCM) and spike timing dependent plasticity (STDP) are the two principal learning behaviors found at cortical synapses. Some BCM induction protocols have been shown to be compatible with STDP rules, thus combining both forms of plasticity. However, we demonstrate that the majority of actual experimental BCM protocols cannot be reproduced by STDP. This sensitivity to spike protocol is inconsistent with the robust BCM behavior generally found in experiments. Moreover, we show that major recent spike timing rules, despite incorporating rate based effects, cannot replicate actual experimental BCM evidence. Thus, the purported convergence between these two important plasticity phenomena is called in question.

1 Introduction

Plastic behavior in synapses exists in a variety of mathematical descriptions, which can be separated in rate- and spike timing dependent effects. Rate effects are mainly represented by the BCM formalism [1], i.e. a transition from weight decrease (long term depression, LTD) to weight increase (long term potentation, LTP) with increase in presynaptic (pre) and/or postsynaptic (post) rate. On the other hand, spike-timing-dependent plasticity (STDP) and its derivations describe weight changes dependent on pre-to-post spike order. In [2], it has been shown that certain forms of STDP can reproduce a BCM curve for a post Poisson rate sweep. Similar Poisson-based transcriptions are used widely in literature, to link computational [3], phenomenological [4] and biophysical [5] STDP models to BCM. In [6], BCM behavior is also shown for STDP if the pre spike is directly interspersed with the post spikes during the rate sweep. However, STDP models seem only to exhibit BCM behavior in exactly these cases, i.e. if a pure rate correlation between pre and post side is assumed and spike-spike correlations are explicitely prohibited [6]. This is in direct conflict with experimental evidence of BCM, where either pre-post spike correlation by itself leads to BCM behavior [7] or where the most reasonable reconstruction of the induction protocol also would imply closely correlated post activity, i.e. a mixture of spike and rate correlation [8, 9]. In extension of [6], we present analytical proof for the incompatibility of the influential STDP model of [2]

*The first two authors contributed equally to this work. The research was supported by funding under the Sixth Research Framework Programme of the European Union, grant no. 15879 (FACETS). J.P. has a doctoral scholarship of the Konrad-Adenauer foundation.

ESANN 2010 proceedings, European Symposium on Artificial Neural Networks - Computational Intelligence and Machine Learning. Bruges (Belgium), 28-30 April 2010, d-side publi., ISBN 2-930307-10-2.

with the BCM protocol of [7] (section 3). Through simulations, we also show in section 4 that two influential recent timing and rate based models [10, 4] cannot reproduce various experimental BCM protocols.

2 Models and protocols

The first model tested for BCM compatibility is [2], i.e. a nearest-neighbor STDP with post reset. The second model [10] is an all-to-all STDP with spike efficacy governed by time-averaged versions of the pre- and post spike train. The third model [4] describes all-to-all and nearest-neighbor STDP with amplitude of the LTP dependent on an additional post spike trace.

The first protocol employed in the test is the correlated BCM of Fig. 8D of [7]. It uses 75 pre-post pulse pairings in 15 groups at a fixed group spike rate λ, swept from 1 to 50Hz. The nominal time for each pre spike is derived from this fixed rate. The pre spike is then uniformly jittered around this nominal time, with the post spike in turn uniformly jittered around the chosen pre spike time[1] (see also Fig. 1). The second protocol represents classical BCM experiments [8], i.e. a 900 pulse pre tetanus swept from 1 to 50 Hz, with the following assumptions for the post side used in this manuscript: The first assumption is a 10 Hz fixed rate Poisson spiking (i.e. only background activity exists, the tetanus has negligible effect on the post side). The second assumption employs a post leaky integrate-and-fire (LIAF) neuron with noisy firing threshold [3], charged by the pre current (which results in a strong correlation between tetanus and post spikes). Parameters for the models of [2] and [10] are the single set published in the respective manuscripts. For the model of [4], parameters have been aligned with the experiments, i.e. the visual cortex set is used for [7] and the hippocampal set for [8].

3 STDP analysis of correlated BCM

In the following, we derive the expected average LTP/LTD of the post-nearest-neighbor STDP of [2] to the BCM protocol of Fig. 8D of [7] as integral over the probability of a given pre-post spike interval multiplied by the weight change for this interval [2]. The grouping of the spike pairings is neglected for this derivation. As outlined above, the interval Δ between the individual pre-post spike pairs has a uniform distribution of $T_x = \pm 10$ms (see also Fig. 1a):

$$f_{T_x}(\Delta) = \frac{1}{2T_x} \quad \text{for} \quad -T_x \leq \Delta < T_x \quad \text{(case 1 and 2 of Fig. 1b)} \tag{1}$$

For case 3 of Fig. 1b, the probability distribution of the interval Δ between a pre spike and the post spike of the next spike pairing is required. Since the pre pulses are also jittered with the above uniform distribution, the convolved overall

[1] The Gaussian distribution documented in [7] is erroneous, according to P. Sjöström, the actual protocol for the experiment was the one outlined above.

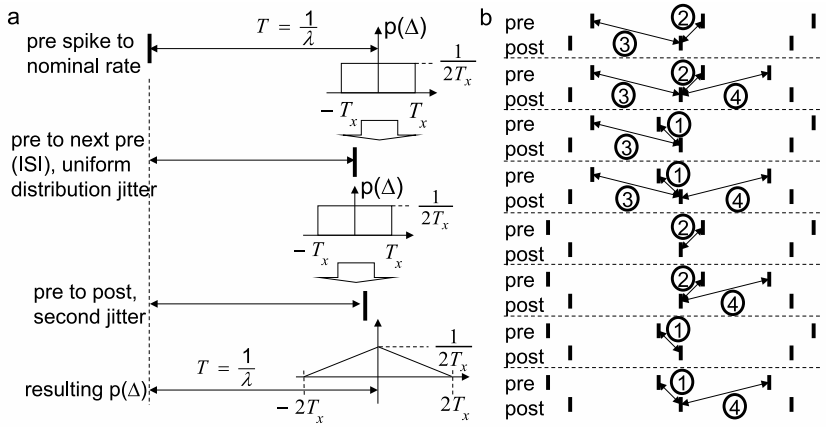

Fig. 1: BCM protocol of [7] a: spike time distributions; b: possible plasticity interactions of this BCM protocol for the STDP model of [2]; note: the regular post-post interval is done for illustrative purposes only.

distribution is triangular with doubled range (see Fig. 1a). This distribution is then shifted by the nominal rate interval T:

$$f_{T_{xx}}(\Delta) = \begin{cases} \frac{\Delta - T + 2T_x}{4T_x^2} & : \quad T - 2T_x \leq \Delta < T \\ -\frac{\Delta - T - 2T_x}{4T_x^2} & : \quad T \leq \Delta < T + 2T_x \end{cases} \tag{2}$$

The interaction of a post spike with the pre spike of the subsequent spike pairing (case 4) follows a similar reasoning. Other spike interactions are not possible for the post reset protocol applied in [2]. The overall weight change $\Delta w(T)$ is then computed as sum over all possible pairings:

$$\Delta w(T) = {}_{(1)}\int_0^{T_x} f_{T_x}(\Delta) \cdot A_+ e^{-\frac{\Delta}{\tau_+}} \mathrm{d}\Delta + {}_{(2)}\int_{-T_x}^{0} f_{T_x}(\Delta) \cdot A_- e^{\frac{\Delta}{\tau_-}} \mathrm{d}\Delta$$
$$+ \frac{1}{2}\left[{}_{(3)}\int_{T-2T_x}^{T+2T_x} f_{T_{xx}}(\Delta) \cdot A_+ e^{-\frac{\Delta}{\tau_+}} \mathrm{d}\Delta + {}_{(4)}\int_{T+2T_x}^{T-2T_x} f_{T_{xx}}(\Delta) \cdot A_- e^{\frac{\Delta}{\tau_-}} \mathrm{d}\Delta \right] \tag{3}$$

The numbers in parenthesis correspond to cases 1 to 4 in Fig. 1b. The LTP and LTD parameters of conventional exponential STDP [2] are denoted by (A_+, τ_+) respectively (A_-, τ_-). The LTD/LTP of the spike pairing itself is split in two integrals for positive (case 1) and negative (case 2) time differences. The two integrals for cases 3 and 4 use the triangular distribution of equ. 2, which is only valid for half the possible interactions, i.e. when the pre spike falls within the interval between its corresponding post spike and the subsequent one (case 3 of Fig. 1b). In this case, the spike is weighted with the LTP portion of the STDP protocol, otherwise its effect on weight change is zero. The plasticity change for case 3 must be split into the two intervals defined by the distribution expression as in equ. 2.

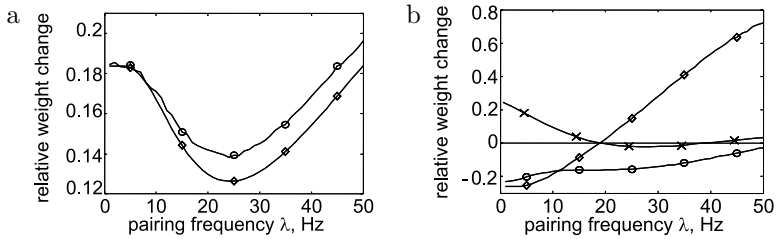

Fig. 2: BCM protocol of [7] as outlined in Fig. 1a for different plasticity models. a: model and parameters of [2], simulated (circles) and analytical solution (diamonds), b: reduced model of [4] for visual cortex data set, nearest neighbor (diamonds) and all-to-all (circles) variants, crosses: model of [10].

$$\Delta w(T)_3 = \frac{1}{2}\int_{T-2T_x}^{T} \frac{\Delta - T + 2T_x}{4T_x^2} A_+ \mathrm{e}^{-\frac{\Delta}{\tau_+}} \mathrm{d}\Delta$$
$$+ \frac{1}{2}\int_{T}^{T+2T_x} \frac{T + 2T_x - \Delta}{4T_x^2} A_+ e^{-\frac{\Delta}{\tau_+}} \mathrm{d}\Delta = \frac{A_+\tau_+^2}{8T_x^2}\mathrm{e}^{-\frac{T}{\tau_+}}\left[2\cosh\left(\frac{2T_x}{\tau_+}\right) - 2\right] \quad (4)$$

Integrating cases 1 and 2 of equ. 3, inserting equ. 4 and its similar LTD counterpart (case 4) in equ. 3 and resubstituting $\lambda = 1/T$ results in:

$$\Delta w(\lambda) = \frac{A_+\tau_+}{2T_x}\left(1 - e^{-\frac{T_x}{\tau_+}}\right) + \frac{A_-\tau_-}{2T_x}\left(1 - e^{-\frac{T_x}{\tau_-}}\right)$$
$$+ \frac{A_+\tau_+^2}{4T_x^2}\cdot e^{-\frac{1}{\lambda\tau_+}}\left(\cosh\left(\frac{2T_x}{\tau_+}\right) - 1\right) + \frac{A_-\tau_-^2}{4T_x^2}\cdot e^{-\frac{1}{\lambda\tau_-}}\left(\cosh\left(\frac{2T_x}{\tau_-}\right) - 1\right) \quad (5)$$

4 Results

We tested the analytical solution of equ. 5 against simulations. Figure 2a shows that both results are in good agreement to each other[2]. The nearest-neighbor STDP model of [2] applied to the BCM protocol of [7] results in LTP only, contrasting with experimental results. This is caused by the narrower, higher-amplitude LTP window compared to LTD, which dominates behavior for the immediate pulse pairings, resulting in an LTP offset independent of the rate (cf. missing λ in the first two terms of equ. 5). With increasing frequency, preceding and successive pulse pairings also contribute to the weight change (the last two terms of equ. 5). Because of the wider LTD window, this first results in reduced LTP at intermediate frequencies and then increased LTP at high frequencies. The same mechanism is present in the Froemke et al. [10] model, with increased

[2]The differences in the weight changes result from the analytically assumed infinite extension of the protocol of Fig. 1 rather than the grouped, burst version described in section 2. The resulting boundary effects reduce LTD interactions for higher rates in the simulation.

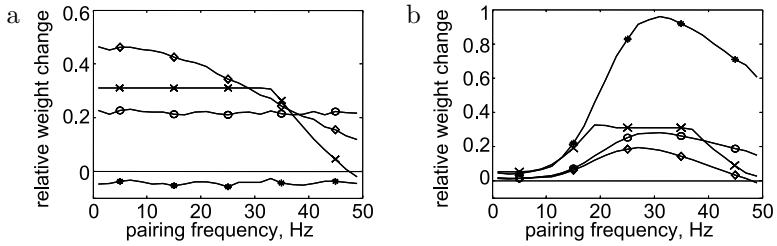

Fig. 3: BCM protocol of [8] for the model of [4] nearest neighbor (diamonds) and all-to-all (circles) variants, models of [10] (crosses) and [2] (stars), a: all models, 10Hz post Poisson spiking; b: post LIAF neuron

LTD at higher frequencies due to the additional post adaptation term (Fig. 2b). The Pfister and Gerstner models [4] are more compatible with the experiments, because they have a highly reduced LTP window for the appropriate parameter set, resulting in LTD at low pairing frequencies. Whereas their all-to-all model reaches LTP only at unrealistically high frequencies, the nearest neighbor implementation is fitting the experimental results well.

For the Dudek and Bear protocol with post Poisson activity, none of the models is able to reproduce the experimental results, as shown in Fig. 3a. The nearest neighbor STDP [2] exhibits no dependence on pre frequency, due to the pairing mode that focuses on the post side. The all-to-all model of [4] shows the same behavior, which in contrast is caused by the cancellation of frequency effects. The nearest neighbor variant results in decreasing LTP with pre frequency, which is opposite to the BCM-like curve found experimentally. The same behavior is shown by the model of [10]; however, the weight is cut-off at lower frequencies due to the hard weight bounds included in the model.

Qualitative behavior changes if we assume correlated post activity, generated by an LIAF neuron (see section 2): All models show only LTP in this case, with a maximum at around 30Hz, cf. Fig. 3b. The increasing LTP is thereby caused by the increasing number of post pulses that are generated with higher pre frequency. As the post pulses are only triggered by pre activity, they follow a pre pulse with a short time interval in the order of the synaptic current's time constant (14ms), resulting in LTP. However, at higher frequencies, the next pre pulse moves into the LTD window of the post spike, resulting in additional LTD, an effect already discussed for the BCM protocol of Sjöström et al.

5 Conclusion

In sum, except for the nearest neighbor Pfister and Gerstner model, no model is able to reproduce any of the BCM experimental results introduced in section 2. Even modern rules which explicitely incorporate a rate component cannot reproduce the majority of rate/BCM experiments (see Fig. 2b and 3). Curiously, STDP type rules, despite being explicitely based on spike-timing and spike-

spike correlations, seem to have considerable trouble reproducing BCM which incorporates significant spike-spike correlations [6], such as the experiments of Fig. 8D of [7] (see Fig. 2). As argued in the introduction, purely rate correlation based BCM transcriptions, despite being inconsistent with biological evidence, seem to be the only method to reproduce BCM behavior for spike-timing rules.

STDP type rules also break down if no post pulses are produced for the region of low pre rate (see Fig. 3b), which results from applying an LIAF neuron or similar reconstructions [9] for the post side. Zero potentation is produced in this case instead of the LTD evident even for subthreshold voltage variations of the post membrane in experiments [11]. Thus, in contrast to this failure of STDP-type rules, biological BCM behavior seems to be replicated across a variety of neuron/synapse operating modes, i.e. its experimental evidence is very robust.

BCM and its derivatives are important ingredients for replicating macroscopic computational and biological effects [1, 12, 13, 9]. STDP on the other hand can explain several microscopic biological effects, such as reinforcement learning or feature classification [3, 5]. Consequently, a rule fulfilling both paradigms would be important to achieve a synthesis of macro- and microscopic neural effects. The investigated spike timing based rules fail in this respect.

References

[1] E.L. Bienenstock, L.N. Cooper, and P.W. Munro. Theory for the development of neuron selectivity: orientation specificity and binocular interaction in visual cortex. *Journal of Neuroscience*, 2(1):32–48, 1982.

[2] E. Izhikevich and N. Desai. Relating STDP to BCM. *Neural Comp.*, 15:1511–1523, 2003.

[3] D. Baras and R. Meir. Reinforcement learning, spike-time-dependent plasticity, and the BCM rule. *Neural Computation*, 19:2245–2279, 2007.

[4] J.-P. Pfister and W. Gerstner. Triplets of spikes in a model of spike timing-dependent plasticity. *Journal of Neuroscience*, 26(38):9673–9682, 2006.

[5] P. A. Appleby and T. Elliot. Synaptic and temporal ensemble interpretation of spike-timing-dependent plasticity. *Neural Computation*, 17:2316–2336, 2005.

[6] D. Standage, S. Jalil, and T. Trappenberg. Computational consequences of experimentally derived spike-time and weight dependent plasticity rules. *Biol. Cybern.*, 96:615–623, 2007.

[7] P.J. Sjöström, G.G. Turrigiano, and S.B. Nelson. Rate, timing, and cooperativity jointly determine cortical synaptic plasticity. *Neuron*, 32:1149–1164, 2001.

[8] S. Dudek and M. Bear. Homosynaptic long-term depression in area CAl of hippocampus and effects of N-methyl-D-aspartate receptor blockade. *PNAS*, 89:4363–4367, 1992.

[9] J. Beggs. A statistical theory of long-term potentiation and depression. *Neural Computation*, 13(1):87–111, 2001.

[10] R. Froemke, I. Tsay, M. Raad, J. Long, and Y. Dan. Contribution of individual spikes in burst-induced long-term synaptic modification. *J. of Neurophysio.*, 95:1620–1629, 2006.

[11] A. Artola, S. Bröcher, and W. Singer. Different voltage-dependent thresholds for inducing long-term depression and long-term potentiation in slices of rat visual cortex. *Nature*, 347:69–72, 1990.

[12] S. Klampfl, R. Legenstein, and W. Maass. Spiking neurons can learn to solve information bottleneck problems and extract independent components. *Neu. Comp.*, 21:911–959, 2009.

[13] M. Garagnani, T. Wennekers, and F. Pulvermüller. Recruitment and consolidation of cell assemblies for words by way of hebbian learning and competition in a multi-layer neural network. *Cognitive Computation*, 1:160–176, 2009.